Electronics and Electrical Engineering

AIMS Electronics and Electrical Engineering, 8(1): 1–27.
DOI: 10.3934/electreng.2024001
Received: 21 November 2023
Revised: 03 January 2024
Accepted: 05 January 2024
Published: 02 February 2024

http://www.aimspress.com/journal/ElectrEng

Research article

Alternating current servo motor and programmable logic controller coupled with a pipe cutting machine based on human-machine interface using dandelion optimizer algorithm - attention pyramid convolution neural network

Santosh Prabhakar Agnihotri* and Mandar Padmakar Joshi

Department of Electronics and Telecommunication Engineering, GES R. H. Sapat College of Engineering Management studies and Research, Nasik, India

* **Correspondence:** Email: spagnihotri@rediffmail.com.

Abstract: The proposed research addresses the optimization challenges in servo motor control for pipe-cutting machines, aiming to enhance performance and efficiency. Recognizing the existing limitations in parameter optimization and system behavior prediction, a novel hybrid approach is introduced. The methodology combines a Dandelion optimizer algorithm (DOA) for servo motor parameter optimization and an Attention pyramid convolution neural network (APCNN) (APCNN) for system behavior prediction. Integrated with a Programmable Logic Controller (PLC) and human-machine interface (HMI), this approach offers a comprehensive solution. Our research identifies a significant research gap in the efficiency of existing methods, emphasizing the need for improved control parameter optimization and system behavior prediction for cost reduction and enhanced efficiency. Through implementation on the MATLAB platform, the proposed DOA-APCNN approach demonstrates a noteworthy 30% reduction in computation time compared to existing methods such as Heap-based optimizer (HBO), Cuckoo Search Algorithm (CSA), and Salp Swarm Algorithm (SSA). These findings pave the way for faster and more efficient pipe-cutting operations, contributing to advancements in industrial automation and control systems.

Keywords: cutting machine; circular saw; servo motor; speed control; position control; pipe length;

proximity sensor

1. Introduction

There is a present surge in the development of homes, apartments, and roads, which raises the need for construction materials, including iron pipes [1]. Building iron retailers must always improve the quality of their services for their customers because of the intense market competition [2,3]. Pipe-cutting operations are available based on the length the customer specifies. Due to the longer working time and potential impact on cutting precision, cutting multiple iron pipes will almost certainly result in decreased cutting efficiency [4]. Automation of pipe-cutting equipment is one effort made to improve cutting production efficiency [5]. A pipe-cutting machine may be run by a PLC or an automated controller. Pipe-cutting machines have seen a remarkable transformation in recent years, owing primarily to improvements in alternate current (AC) servo motor technology and the integration of sophisticated PLC-based control systems with user-friendly HMI [6].

This technological convergence has heralded a new era of accuracy and efficiency in pipe fabrication and production operations. AC servo motors, which provide precise control over cutting processes, are at the heart of this change [7]. These motors deliver strong torque, quick response times, and remarkable accuracy, guaranteeing that each cut is completed precisely [8,9]. Their ability to maintain constant speed and position control under varied load situations makes them excellent for applications requiring precision. In addition to the AC servo motors, PLCs act as the cutting machines' brains. They make difficult-cutting jobs easier to automate by executing pre-programmed instructions. PLC is adaptable and versatile, allowing for adaptation to meet unique production needs. They guarantee that numerous machine components, such as servo motors, sensors, and cutting tools, work in unison, resulting in optimum cutting operations [10]. The HMI component of these devices is critical to improve usability and operator control. HMI systems offer a user-friendly interface that enables operators to easily monitor and manage the machine's functionality. Touch-screen displays, simple software, and real-time feedback allow operators to quickly configure parameters, alter settings, and resolve difficulties.

This user friendly interface additionally shortens the learning curve for operators, but it also lowers downtime, enhancing production as a whole [11]. The most recent generation of pipe-cutting machines with AC servo motors and PLC-based HMI systems marks an industrial-technological paradigm change [12]. These machines combine precision, speed, and ease of use, making them important tools in a variety of sectors, such as construction, automotive, and aerospace [13,14]. As technology advances, we may expect even more novel features and capabilities, improving the field of pipe cutting and automation in factories [15]. A comparison of literature reviews is shown in Table 1.

The major contributions of this work are summarized as follows:

- Automatic pipe-cutting machines reduce dependence on manual labor, and there is the potential for cost savings and improved safety in the industrial sector.
- The automatic control of the pipe-cutting machine, facilitated by a servo motor and PLC, ensures high-speed and high-output operations, contributing to efficient production processes.

- Recognizing the inherent challenge of subpar cutting efficiency when dealing with numerous iron pipes, the proposed approach focuses on automation, thereby enhancing overall production efficiency.
- The servo motor's excellent response and precision make it ideal for placement. It is a motor that can precisely control speed, torque, and rotational angle. For great accuracy and precision in pipe cutting, a servo motor with PLC should be used.

The remainder of the paper is as follows: Section 2 reviews the literature and motivation for the present work. Section 3 describes automatic pipe-cutting devices based on HMI, PLC, and servo motors. Section 4 illustrates the DOA-APCNN approach. Section 5 demonstrates the results and discussion. In Section 6, the paper concludes.

Table 1. Comparison of literature reviews.

Reference	System Description	Advantages	Disadvantages	Used Methods
Shaheed and Selman [16]	PLC-based automatic control for steel plate cutting. Encoder for length specification, HMI for monitoring.	Improved automation, precise control with PLC and Encoder.	Dependency on PLC, potential complexity in maintenance.	PLC, Encoder, HMI
Zhu et al. [17]	Cutting device with two servo motors using Archimedes spiral. High automation, low disturbance, and accurate control.	A high degree of automation, and low disturbance in cut surface.	Complexity in setup and maintenance, potential cost.	Servo motors, Archimedes spiral
Zhu et al. [18]	Relationship model for cutting blade feed speed and force. Genetic algorithm-optimized fuzzy PID control.	Constant cutting force, and optimization for the control scheme.	Complexity in model development, dependency on optimization.	Matlab, Genetic algorithm, Fuzzy PID control
Du et al. [19]	AT-TENG for power generation using drill pipe-embedded annular design.	Harvesting energy from arbitrary direction vibrations.	Limited information on practical applications, and potential wear.	Triboelectric nanogenerator, Annular design
Mu et al. [20]	Robotic arm-driven knife for object cutting. Position, force, and impedance controls.	Adaptive control for evolving contacts, estimation of physical parameters.	Complex control system, reliance on sensing technology.	Robotic arm, Position, Force, Impedance controls, Force sensing
Limonov et al. [21]	Study of dynamics of electric drive with cyclic action of flying saw in pipe welding mill.	Improved dynamic performance, and reduction in position error.	Limited information on specific improvements, and potential complexity.	Electric drive, Dynamic performance analysis
M. Salemet al. [22]	Wind tunnel-tested 0.8m-diameter pitch-controlled wind turbine model. Neural network pitch control.	Effective pitch angle control is practical for small wind turbines.	Limited information on real-world applications, and potential complexity.	Wind tunnel testing, DC servo-motor, Neural network pitch control

2. Recent research work: A brief review

The control of servo motors using a variety of approaches and factors was the subject of several earlier research papers that may be found in the literature. Some of them are reviewed here.

Shaheed and Selman [16] presented a programmable logic controller (PLC)-based automated control system for a steel plate cutting machine that was previously operated manually in a factory. The system included an encoder that communicates with the PLC to define the length of the steel plate to be cut. The system operator finished the system operation by monitoring and controlling the system performance using a human-machine interface (HMI) unit.

To attain a high level of automation, Zhu et al. [17] created a novel cutting device that makes use of two servo motors. It ensured little disruption of the cut surface and offered precise process control by using the Archimedes spiral. Furthermore, hydrate samples of any length may be cut with almost no chips in a short amount of time thanks to the sample long-stroke push unit's functioning. Zhu et al. [18] presented the relationship model between the force of cutting and the cutting blade feed speed developed using MATLAB, based on the link between blade feed and cutting force discovered via cutting trials, in addition to the mathematical model of the cutting head's rotation and blade feed movement. To maintain the blade's cutting power throughout the cutting operation. The fuzzy proportional-integral-derivative control was optimized using a genetic algorithm, and the electric drive downhole tubing cutting tool's automated control system was built. The cutting force control simulation of the tube cutting process was performed using MATLAB/Simulink. The effectiveness of the genetic algorithm-optimized fuzzy proportional-integral-derivative control was contrasted with that of other conventional controllers.

Du, et al. [19] suggested using annular silicone rubber and two electrodes to make up the drill pipe-embedded annular-type triboelectric nanogenerator. To achieve power generation, the architecture of AT-TENG enabled the silicone rubber to readily come into touch with and separate from the electrodes in a small area under arbitrary direction vibration.

Mu, et al. [20] investigated the three steps that a robotic arm used to drive a knife into an item, which were pushing, slicing, and touching. Position, force, and impedance controls function alone or in concert, aided by force sensing and/or based on fracture mechanics, to handle changing contacts with the material and cutting board. This allows the knife to split the item along a predetermined trajectory. Physical characteristics associated with cutting were estimated for each item using force data collected during the pressing phase. These predicted values are immediately employed to carry out the slicing step for control purposes.

Limonov et al. [21] developed the dynamics of the electric drive with the cyclic action of a flying saw in an electric pipe welding mill. Alternatives for enhancing this electric drive's dynamic performance were taken into account. The suggested ways to make the cyclic action mechanism move more smoothly decreased the mechanism's position error in both moving and stationary states.

A wind tunnel was constructed, built, and tested by Salem et al. [22]. A miniature pitch-controlled wind turbine model with a diameter of 0.8 m was also made. The pitch angle was controlled by a linkage system that employed a DC servo motor as the actuator. It operated faultlessly and was shown to be efficient and useful for tiny wind turbines. This research aimed to achieve two principal goals. First, take particular note of the features of the kind of tiny wind turbine that was being evaluated at different pitch angles and wind speeds (WSs). Second, a pitch angle control mechanism was installed to regulate the amount of power the turbine generated at wind speeds that were higher than its rated speed. The neural network matching function of the pitch angle control system regulates the pitch angle in a way that makes the required power curve achievable for the wind turbine.

2.1. Motivation for the present work

The research works discussed in the literature review offer innovative solutions for various servo motor control applications, but they also come with certain drawbacks. These disadvantages are mostly related to complexity, expense, and maintenance issues. The complicated control systems and hardware components required can be costly to design and maintain, making them inaccessible for smaller-scale projects or situations with limited resources. Furthermore, the complexity of these systems can contribute to increased breakdown risks and maintenance requirements, especially in industrial settings where downtime is costly. Scalability can also be an issue, particularly for systems like the waste management setup, which may struggle to scale to bigger installations. Furthermore, the energy consumption of these high-precision control systems may be large, posing a possible concern for energy efficiency. Finally, deploying and operating these advanced technologies may require specialist knowledge, increasing the total cost and complexity of their adoption. Despite these disadvantages, these research papers add essential insights and advances to the field of servo motor control, paving the way for breakthroughs in automation and precision control applications. The goal of addressing these drawbacks has inspired the present work.

3. Configuration of AC servo motor and PLC coupled with a pipe cutting machine based on HMI

Figure 1 shows the configuration of an automatic pipe cutting device based on HMI, PLC, and servo motor. Push buttons and proximity sensors are utilized as input devices for the PLC. The system is turned on and off using a push-button. Pipes are discovered using a proximity sensor. Servo motors and relays are operated by the PLC's output signal [23]. The encoder that detects motor movement and the motor itself make up the two main parts of an AC servo motor. By using proximity, a pipe's presence can be determined. The length of the pipe can be calculated by knowing how many rotations the AC servo motor completed via the encoder. Digital encoders with absolute sensors are utilized in servo motors [24–27]. Perfect encoders, as opposed to incremental encoders, are made to detect rotation angles as precisely as feasible. Calibration cannot therefore be done each time you operate. Even when the power is abruptly cut off, the absolute encoder maintains the motor shaft rotation's track position. In the event of a power switched-off rotation takes place seamlessly. The servo-motor is controlled by the ac-servo drives, also referred to as servo amplifiers, in accordance with the PLC positioning module's command signal instructions [28–30]. To minimize the discrepancy between the input and the feedback signals from an encoder, the AC servo drive will process the error signal while operating. This will enabled the servo drive to keep an eye on the performance of the AC servo motor and address any issues that may come up. The servo amplifiers' power amplifiers boost the signal to make it more powerful so that the AC servo motor can move it, and the comparator checks for false signals. Position mode, speed, and torque of an AC servo motor can all be altered individually or in combination to accommodate user preferences [31–33]. The relay controls the saw circle, the indicator lights, and the AC motor. In order to prevent the pipe from trembling while being cut, the AC servo motor advances cutting blades, pulls pipes, and clamps pipes. Pipes are cut using the circular saw motor. Pipe cutting is done by first setting up the pipe size, quantity, and length, and then inputting the pipe manually. The pipe will then start moving independently after that. When the pipe reaches the required length, it will be sliced and clamped.

The HMI can be used to administer and monitor the system's work process [34,35]. The proposed DOA approach is used to control servomotor position, speed, torque and APCNN is used to predict the servo motor control by this hybrid approach to get high performance and low cost productivity.

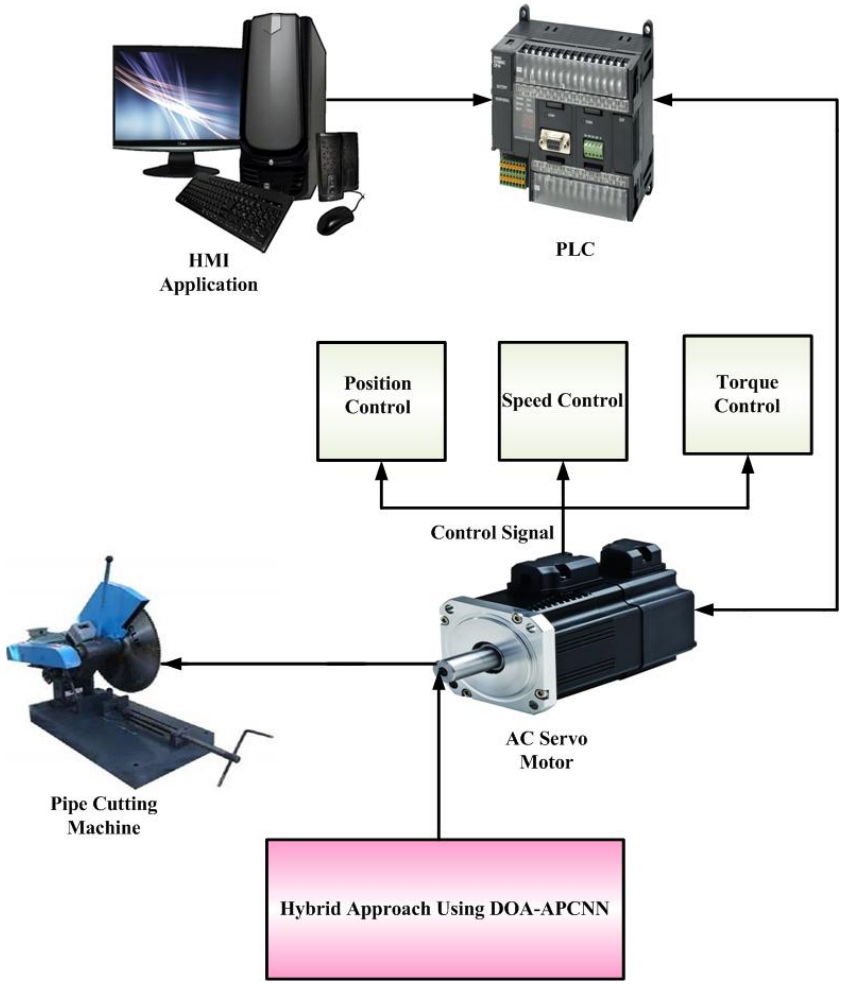

Figure 1. Configuration of AC servo motor and PLC coupled automatic pipe cutting machine based on HMI.

3.1. Pipe cutting machine

Hardware components of the pipe-cutting device comprise a servo drive, AC servo motor, encoder, push button, and proximity sensor. The pipe-cutting machine automatic controllers, which include central processing units, are PLCs.

Figure 2 shows the structure of pipe-cutting machine. Push buttons and proximity sensors are utilized as input devices for the PLC. The system is turned on and off using a push-button. Pipes are found using a proximity sensor [36]. Servo motor drives and relays are controlled by the PLC's output signal. The servo drive powers the AC servo motor, and the encoder monitors motor rotation so that the length of the pipe that has to be cut may be determined by counting the motor spins [37].

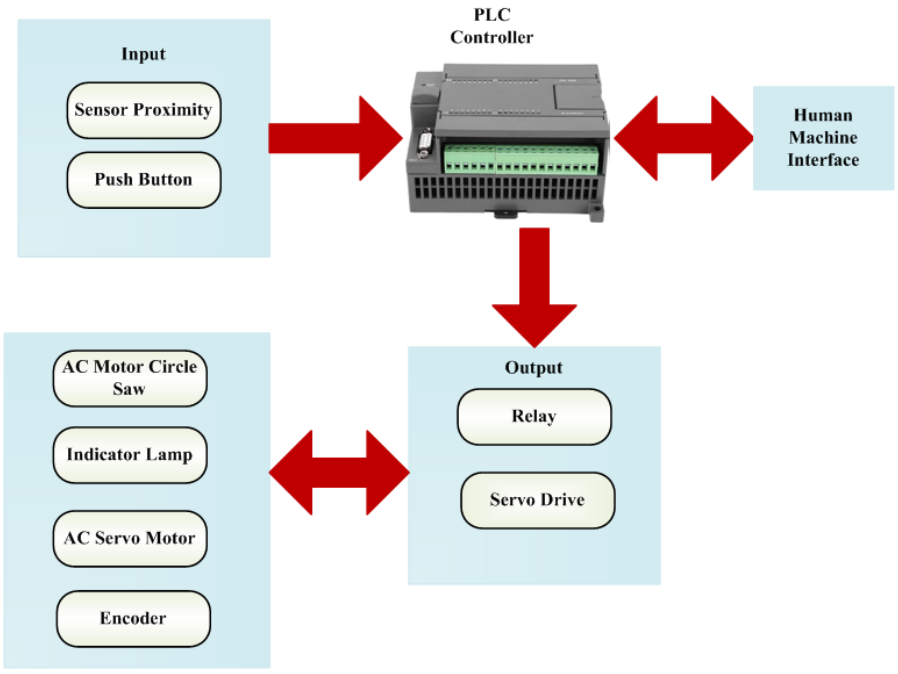

Figure 2. Structure of pipe-cutting machine.

3.1.1. Pipe cutting model

When the circular saw teeth make interaction with the pipe, a cutting force is applied. Therefore, determining the interaction area and locating the circular saw teeth there are essential.

$$D = \sqrt{\left(z_q - z_d\right)^2 + \left(y_q - y_d\right)^2} \tag{1}$$

$$\theta_{OUT} = bCOS\left(\frac{D^2 + r^2 - R_0^2}{2DS}\right) \tag{2}$$

$$\theta_{IN} = bCOS\left(\frac{d^2 + r^2 - R_j^2}{2Ds}\right) \tag{3}$$

$$\phi = bSIN\left(\frac{\left|y_q - y_d\right|}{D}\right) \tag{4}$$

Where, D indicates the separation between the pipe's and the circular saw's center points; r indicates circular saw's diameter; R_0 indicates pipe's outside radius; R_j indicates pipe's inner radius. Additionally, the following definitions can be used to describe each tooth's position when the circular saw is rotating:

$$\theta_L\left(N,T\right) = \frac{N2\pi}{n} + \omega T \tag{5}$$

$$\theta_T(N,T)=\theta_L(N,T)-\left\lfloor \frac{\theta_L(N,T)}{2\pi} \right\rfloor 2\pi \tag{6}$$

Where, N indicates the tooth's index; $\theta_L(N,T)$ indicates each tooth's inclination in relation to the positive axis; n indicates amount of teeth overall; ω indicates the circular saw's angle of rotation; $\lfloor \bullet \rfloor$ indicates functional floor. The following can be used to determine whether the circular saw teeth are among the interaction region:

$$\text{When } \begin{Bmatrix} 2\pi-(\varphi+\theta_{OUT})\le\theta_T(N,T)\le 2\pi-(\varphi+\theta_{IN}):n_T(N,T)=1 \\ 2\pi-(\varphi-\varphi_{IN})\le\theta_T(N,T)\le 2\pi-(\varphi-\varphi_{OUT}):n_T(N,T)=1 \\ Otherwise:n_T(N,T)=0 \end{Bmatrix} \tag{7}$$

Wherever, $n_T(N,T)$ indicates the variable for each circular tooth; 1 denotes true, while 0 denotes false. The following is an expression for each tooth's cutting force:

$$f_d(N,T)=n_t(N,T)\frac{\tau_h X\, 2\pi w_F Sin(\theta_T(N,T))}{\omega n \sin(\varphi_a)\cos(\varphi_a+\beta_F-\alpha_k)} \tag{8}$$

Where, τ_h indicates shear stress on the pipe's material; X indicates circular saw thickness; w_F indicates feed speed; φ_a indicates shear angle, β_F indicates angle of friction; α_k indicates angle of rake, the tangential force and normal force components of the cutting force in Equation (8) are along these lines,

$$f_T(N,T)=f_C(N,T)\cos(\beta_F-\alpha_R) \tag{9}$$

$$f_T(N,T)=f_C(N,T)\sin(\beta_F-\alpha_R) \tag{10}$$

In Cartesian space, the contact force of pipe-cutting is eventually defined as follows:

$$f_X(N,T)=f_T(N,T)\sin(\theta_T(N,T))+f_N(N,T)\cos(\theta_T(N,T)) \tag{11}$$

$$f_Y(N,T)=f_T(N,T)\cos(\theta_T(N,T))-f_N(N,T)\sin(\theta_T(N,T)) \tag{12}$$

$$f_X(T)=\sum_{N=1}^{n} f_X(N,T) \tag{13}$$

$$f_Y(T)=\sum_{N=1}^{n} f_Y(N,T) \tag{14}$$

3.2. Modeling of AC servo motor

AC servo motors employ AC electrical input to create mechanical output in the form of accurate angular velocity. Encoders are used to control AC servo motors, which are AC motors. The stationary

component of the motor is called the stator and then the rotating component of motor is known as rotor. These servo motors are controlled by controllers that offer closed-loop control and feedback. They are renowned for their remarkable precision and controllability. The system model includes an inertia load connected to the motor's output shaft as well as a two-phase AC servo motor. The mechanical system's dynamic equation was as defined in Eq (15).

$$\tau_c = \tau_l + C_m\theta(T) + I_m\ddot{\theta}(T) \tag{15}$$

Where, τ_c indicates torque control; τ_l indicates mechanical load; C_m indicates motor friction coefficient; θ indicates motor angular position; I_m indicates the motor's moment of inertia; $\ddot{\theta}$ indicates the motor's angular acceleration. The AC servo motor's control torque was provided by

$$\tau_c = J_1W(T) - J_2\dot{\theta}(T) \tag{16}$$

Wherever, J_1 and J_2 indicates motor constant; W indicates input rated voltage; $\dot{\theta}$ indicates the motor's angular velocity. The mechanical load torque is given as

$$\tau_l = C_l\theta(T) + K_l\ddot{\theta}(T) \tag{17}$$

Where, C_l indicates the friction coefficient, and K_l indicates the load's moment of inertia.

The equation that results from combining (15) and (16) is (18).

$$\tau_l + C_m\theta(T) + I_m\ddot{\theta}(T) = J_1W(T) - J_2\dot{\theta}(T) \tag{18}$$

By substituting (17) into (18),

$$C_l\theta(T) + K_l\ddot{\theta}(T) + C_m\theta(T) + I_m\ddot{\theta}(T) = J_1W(T) - J_2\dot{\theta}(T) \tag{19}$$

The equation becomes (20) after applying the Laplace transform to (19).

$$C_lu\theta(u) + K_lu^2(u) + C_mu\theta(u) + I_mu\theta(u) = J_1W(u) - J_2u\theta(u) \tag{20}$$

The final equation was (21) comes after adjusting for (6).

$$J_1W(u) = C_lu\theta(u) + I_lu^2\theta(u) + C_mu\theta(u) + I_mu^2\theta(u) + J_2u\theta(T) \tag{21}$$

The motor transfer function between $\theta(u)$ and $W(u)$ was obtained.

$$J_1W(u) = \left(I_mu^2 + K_lu^2 + C_mu + J_2u\right)\theta(u) \tag{22}$$

By modifying Eq (22),

$$\frac{\theta(u)}{W(u)} = \frac{J_1}{(I_m + I_l)u^2 + (C_m + C_l + J_2)u} \tag{23}$$

Equation (23) could be further modified as

$$\frac{\theta(u)}{W(u)} = \frac{J_1}{u\left[\left(I_m + C_l + J_2\right)\left(\frac{\left(I_m + I_l\right)u}{I_m + C_l + J_2} + 1\right)\right]} \tag{24}$$

The gain and time parameters for the system are displayed underneath the gain parameter.

$$\text{System gain parameter} = J_p = \frac{J_1}{C_m + C_l + J_2} \tag{25}$$

$$\text{System time parameter} = \tau_p = \frac{J_m + J_l}{C_m + C_l + J_2} \tag{26}$$

Equations (25), (26), and (27), which are shown in Eq (27), were substituted into Eq (24), to create the model of the AC servo motor.

$$\frac{\theta(u)}{W(u)} = H_m(u) = \frac{J_p}{u\left(\tau_p u + 1\right)} \tag{27}$$

The system parameters J_p and τ_p were each given a random signal disturbance. The random signals modified the system parameter values, and then the updated internal model control received the revised values. Constant values were added to the random signals to compensate for the motor parameter values' constant limitations and keep them nominal or close to an average point. AC servo motor control is shown in Figure 3.

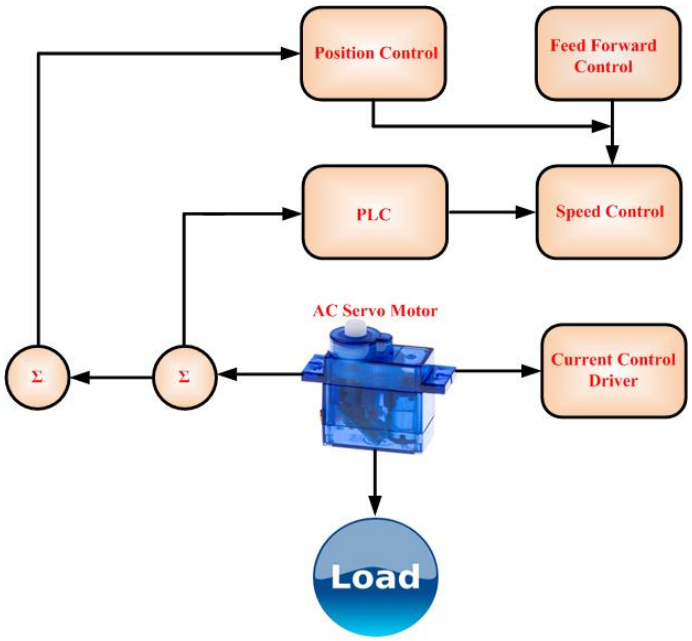

Figure 3. Schematic representation of AC servo motor control.

3.3. Programmable logic controller

PLCs are ruggedized industrial computers that are used to run production processes like

assembly lines, robots, machines, or any other task that needs high reliability, simple programming, and process fault detection. There are now several original equipment manufacturers offering options for considerations in the selection of a suitable PLC. One system from one manufacturer may be superior or more economical than another for a specific necessity, function, or input/output. The quantity of inputs/outputs, digital I/O, required memory capacity, CPU speed and power requirements, coding instructions, manufacturer's service support, and other critical factors must all be considered when choosing the ideal PLC for an automation operation. All of these qualities are connected, and a court decision must be made. The basic components of the PLC are a CPU, memory, and I/O modules for handling input and output data. Basic structure of the PLC is displayed in Figure 4.

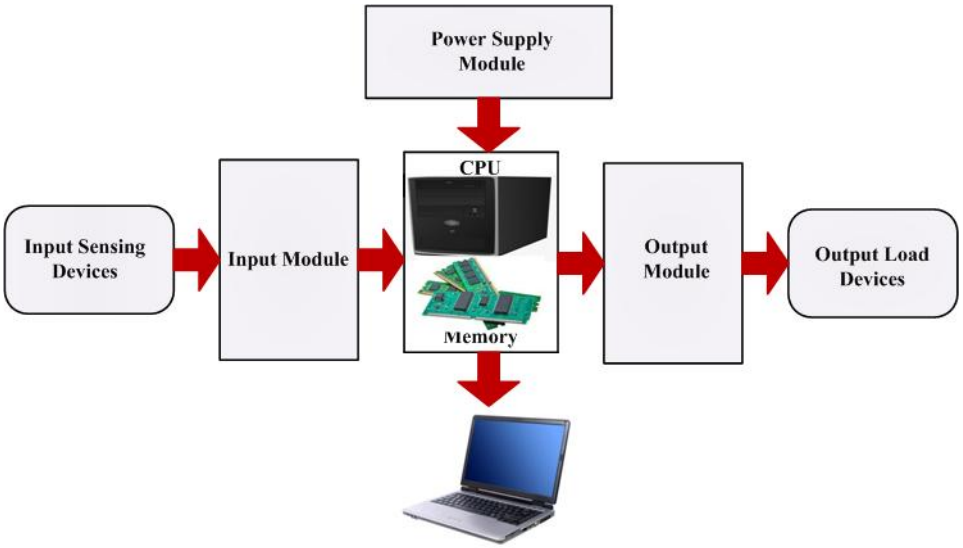

Figure 4. Structure of PLC.

3.4. Objective function

Four mechanisms were used to get the lowest possible production cost. Cost of handling the component in terms of time c_{TP}. The cost rate c_r for the amount of time required to load and unload the pipe to be cut p_T was established as a result.

$$c_{TP} = c_r . p_T \tag{28}$$

3.4.1. Cost of machining time

A full cycle of the finished product, designated as f_p, and the cost rate, denoted as c_r, were used to evaluate the machining time.

$$c_{MT} = c_r . f_p \tag{29}$$

3.4.2. Cost of time in tool changeover

The cost rate c_r, the minutes-per-cut saw changeover time t_S, and the quantity of finished

machined components N_M served as the three determining variables.

$$c_{TC} = c_r.(t_S / N_M) \tag{30}$$

3.4.3. Tool cost per unit

The cost of tool c_T was listed in [$], and the total number of completed machine components N_P are given in units.

$$c_{cpu} = (c_T / N_P) \tag{31}$$

As a result, one can estimate the cutting speed that results in the lowest cost per piece by deriving with respect to v and using an equation equal to 0 in Eq (31).

$$c_{pp} = C\left(\frac{N}{1-N}.\frac{C_0}{C_0 + C_T}\right) \tag{32}$$

4. Servo motor and PLC coupled with pipe cutting machine based on HMI using DOA-APCNN approach

In this paper, the DOA-APCNN approach is proposed to optimize the control of a servo motor by adjusting parameters like motor speed, position, or torque, where all are maximizing the performance based on an objective function. The APCNN method is used to predict the servo motor control system. The operation procedure of DAO-APCNN is given below.

4.1. Dandelion optimizer algorithm (DOA)

The dandelion optimizer's mathematical equation is thoroughly explained in this section. The DOA is a nature-inspired optimization method based on the behavior of dandelion seeds. It has demonstrated promising results in improving the performance of different systems and has been effectively used to a variety of optimization challenges. Three phases make up the long-distance flight: rising, descending, and landing. DOA method includes the following steps. The flowchart of DOA is shown in Figure 5.

Step 1: Initialization

Initialize the input position, speed, and torque of the servo motor.

Step 2: Random generation

Each feasible solution is generated randomly using the upper and lower bounds of the given drawback, and the ith individual X_i is represented as

$$X_i = rand \times (UB - LB) + LB \tag{33}$$

Here, *rand* indicates a random number among [0, 1].

Step 3: Fitness function

$$F = Min(obj) \tag{34}$$

Step 4: Rising stage

The wind speed and weather, which determines whether it is sunny or rainy during the rising phase, both affect how high dandelion seeds rise.

Case 1: Because wind speed has a log-normal distribution, dandelion seeds are more likely to travel long distances on sunny days. The DOA so strongly emphasizes exploration on sunny days. The WS continuously alters the vortex over the dandelion seeds, sending them spiraling upward. The following is a description of the dandelion seed spiral model:

$$X_i^{t+1} = X_i^t + \alpha * s_x * s_y * 1nY * (X_s^t - X_i^t) \tag{35}$$

$$X_s^t = rand(1, Dim) * (UB - LB) + LB \tag{36}$$

$$\alpha = rand() * (\frac{1}{T^2} t^2 = \frac{2}{T} t + 1) \tag{37}$$

$$r = \frac{1}{e^\theta} (38)\, S_x = r * \cos\theta \tag{38}$$

$$S_y = r * \sin\theta \tag{39}$$

Here, X_i^t indicates seed location at iteration time t; X_s^t indicates the location of the dandelion seed selected at iteration t; T indicates extreme number of iterations; In Y indicates logarithmic distribution subject to $\mu = 0, \sigma^2 = 1, \alpha$ is an adaptive parameter. The component coefficients of the lift of dandelion seeds are represented by S_X and S_y, and $\hat{I}$ is a random number in $[-\pi, \pi]$.

Case 2: On days when it has rained, dandelion seeds cannot efficiently rise with the breeze. Dandelion seeds currently draw attention to exploitation in the neighborhood. The formula and associated model are shown below:

$$e = T^2 - 2T + 1 \tag{40}$$

$$\beta = 1 - rand() * \frac{1}{e}(t^2 - 2t - 1) \tag{41}$$

$$X_i^{t+1} = X_i^{t+1} * \beta \tag{42}$$

Here, β indicates the local dynamic parameter, and T indicates the extreme number of iterations.

In conclusion, the following equation represents the ascending phase of dandelion seeds:

$$X_i^{t+1} = \begin{cases} X_i^t + \alpha * S_x * S_y * 1nY * (X_s^t - X_i^t) \; randn < 1.5 \\ X_i^t * \beta_{else} \end{cases} \tag{43}$$

Here, *randn* represent the random number with a normal distribution. DO place a strong emphasis on worldwide discovery throughout this period. The dandelion population can move to the desirable location for reproduction while reflecting the stability of the decrease by utilizing the average

position following the rising phase. The following is the mathematical equation for the falling phase:

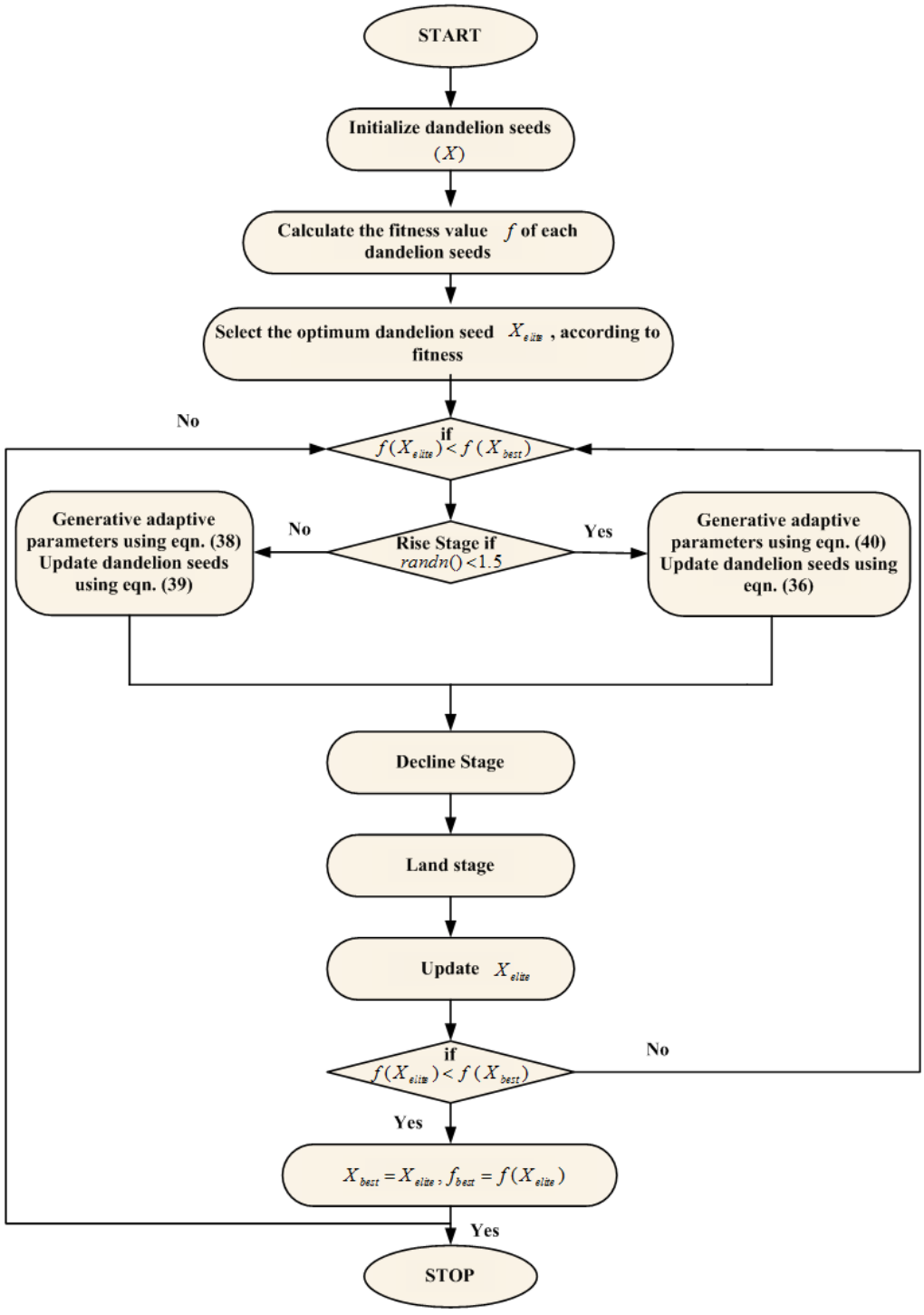

Figure 5. Flowchart of DOA.

Step 5: Descending stage

DO place a strong emphasis on world-wide discovery throughout during the landing phase. By applying the average position following the increasing phase, the dandelion population can move to

the best site for reproduction while also representing the stability of the reduction. The mathematical equation for the corresponding falling phase is described as:

$$X_{mean-t} = \frac{1}{pop}\sum_{i=1}^{pop} X_i \tag{44}$$

$$X_i^{i+1} = X_i^t = \alpha * \beta_t * (X_{mean-t} = \alpha * \beta_t * X_i^t) \tag{45}$$

In the i[th] iteration, X_{mean-t} represents the normal location of the dandelion population. Brownian motion is β_t .

Step 6: Landing stage

DO concentrate on local neighborhood development throughout the landing phase. In accordance with the stages of rising and falling, the dandelion seeds choose their landing location at random. Local information about the current elite seed is used to get closer to the global optimum. The landing stage is represented mathematically as follows:

$$X_i^{i+1} = X_{elite} + levy(\lambda) * a * (X_{elite} - X_i^{t+1} * \delta) \tag{46}$$

$$\delta = \frac{2t}{T} \tag{47}$$

Here, X_t indicates best seed location at the time of iteration *t*; *T* indicates the extreme number of iterations; $levy(\hat{I} >>)$ indicates the Levy flight function; $\hat{I} >>=1.5$, $\hat{I}$ indicates linear rising between [0,2].

Step 7: Updating process

In the updating process, update the best solutions of the above iterations.

Step 8: Termination criteria

In the termination criteria, if it is met, the best solution has been found; if not, repeat the procedure.

4.2. Attention pyramid convolution neural network (APCNN)

In this section, attention pyramid convolution network (APCNN) is optimized to promote college english independent learning [38]. A pyramid convolution attention network is proposed to efficiently capture long-term dependence and combine features from different levels to solve semantic segmentation problems. The pyramid of attention (PA) network is a fresh framework developed for digital image processing.

On the other hand, the convolution neural network (CNN) by the following $\{b_1, b_2, ..., b_3\}$ are considered, where $b_1, b_2, ...b_3$ are denoted as number of blocks. APN generates *m* equivalent feature hierarchy by following $\{a_m, a_{m+1}, ...a_{m+M-1}\}$. By paying closer attention a pyramidal hierarchy with two characteristics, namely pyramidal channel attention, is established, embedding channel correlations. Also, in a second bottom-up conduit, local information is delivered from lower to higher pyramid levels as well as pyramidal spatial attention, which locates to discriminative regions from

various scales based on $\left\{a_m^{(SP)} + a_{m+1}^{SP}, \ldots\ldots a_{m+M-1}^{SP}\right\}$ and $\left\{a_m^{CP} + a_{m+1}^{CP}, \ldots\ldots a_{m+M-1}^{CP}\right\}$. Where, a indicates attention pyramid, SP represented the pyramidal spatial attention, and CP denoted pyramidal channel attention. A spatial attention mask a_N^{SP} is produced using the relevant feature map as input, fm_N. To compress spatial information, each feature map is sent through a de-convolution layer with one output channel. Finally, using the sigmoid function, each component of the spatial notice mask is normalized to the interval to indicate the spatial importance by following Eq (48).

$$a_N^{SP} = \sigma\left(\vartheta_{CP} * fm_N\right) \tag{48}$$

Where, σ denotes the sigmoid function; $*$ indicates deconvolution; ϑ_{CP} indicates convolution kernel. The channel attention pyramid is derived from the matching feature map in the feature pyramid using global average pooling and two completely linked layers. The following Eq (49) represents the channel attention mask.

$$a_N^{CP} = \sigma\left(w_2 \cdot rl\left(w_1 \cdot GAP\left(fm_N\right)\right)\right) \tag{49}$$

Where, GAP (·) indicates the pooling function for the global average by following equation (50).

$$GAP\left(fm_N\right) = \frac{1}{S \times D} \sum_{a=1}^{D} \sum_{b=1}^{S} fm_N(a,b) \tag{50}$$

Here, σ and rl indicate the Rely function and the sigmoid, respectively; multiplication of elements is represented by the dot product; S and D indicate the spatial dimensions of fm_N; w_1 and w_2 indicate two fully-connected layers' weight matrices. Equation (51) can be used to classify data by using the learnt attentions to weight features (fm_N) and obtaining fm'_N .

$$fm'_N = fm_N \cdot \left(a_N^{SP} \oplus a_N^{CP}\right) \tag{51}$$

Where $\oplus$ represents the addition operation and the structure of APCNN is shown in Figure 6. Finally, APCNN achieves a high efficiency and reduced error quantities.

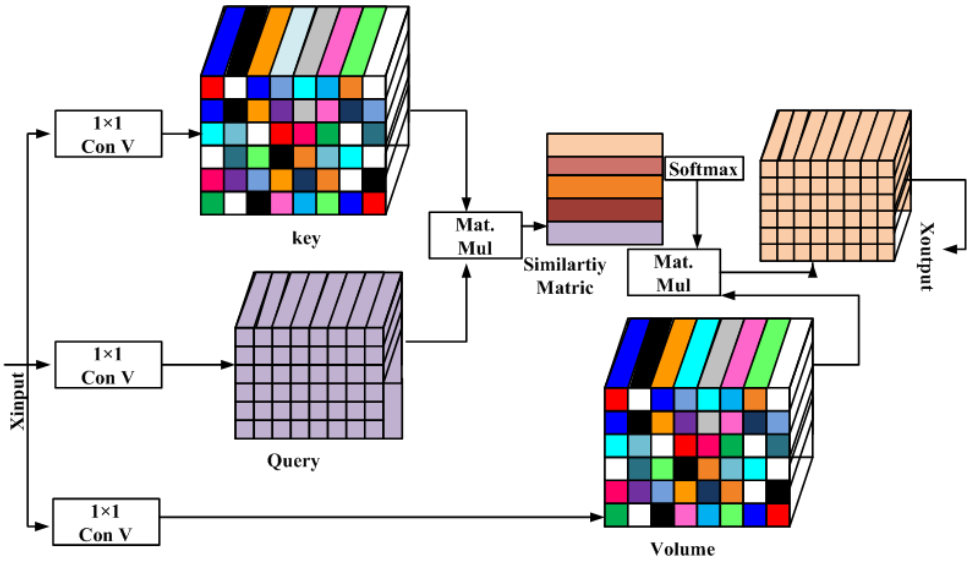

Figure 6. Attention pyramid convolution neural network.

5. Result and discussion

The results of the proposed servo motor and PLC with pipe cutting machine based on HMI are discussed here. This work can be done by solving the optimization problem such that the cost will be minimized for the system and enhance the production efficiency by automating pipe cutting processes, resulting in precise and consistent outcomes. The proposed technique is implemented on the MATLAB platform, and compared with existing methods such as HBO, CSA, and SSA.

Figure 7 depicts the pipe cutting machine force. The pipe cutting machine force is related to the time and it increases the performance of the machine. Initially, the pipe cutting force is -180 N and it reduces to -720 N in 60 s and increases in the same time duration. The cutting force remains constant from 70 s to 370 s when the cutting force is -375 N, after the pipe cutting force reduces to -950 N in the same time duration and the cutting force increases to -10 N in 400 s. The position of the pipe is 0.5 rad and the pipe is moved to 75 rad in 2.5 s and the pipe reaches 135 rad in 3.5 s as the pipe movement is based in the servo motor control signal after the cutting machine cut the pipe as is shown in Figure 8(a). The maximum velocity of the servo motor is 40 rad as is shown in Figure 8(b). The maximum acceleration is 200 rad/s^2 and the minimum acceleration is -150 rad/s^2 as is shown in Figure 8(c). The effectiveness of the proposed controller is resistance to disturbances. The disturbance starts from 0 to 0.4 Nm in 1.25 s and it decreases to 0 similarly in the second and third cycle of the disturbance as is shown in Figure 9. Robustness of the servo motor control based on the tracking position of the presence of the pipe and position of the pipe is 4.2 rad in 0.25 s and the servo motor proximity sensor analyzes the presence of the pipe. In second cycle, the position of the pipe is 10.1 rad in 0.7 s. Subsequently, the position moves to 14 rad in 1.2 s, followed by another movement to 16 rad in 1.7 s. Afterward, the pipe position advances to 17.5 rad in 2.2 s, and finally, the position reaches 18.1 rad in 2.7 s. The pipe reaches 19 rad in 3.2 s, and then the position advances to 19.3 rad in 3.7 s. Subsequently, the position further moves to 19.5 rad in 4.2 s. After the pipe position reaches 17.7 rad at 4.7 s, the position is shown in Figure 10.

The control input is provided to the pipe cutting machine by the servo motor. The position tracking errors are compared with Sliding Internal Mode Control (SIMC) – Sliding Mode Control (SMC). The control input signal increases and remains constant at 0.25 Nm from 1 to 2.5 s. Afterward, the control input signal decreases to 1.7 Nm in 2.7 s, and then the control input signal remains constant. In the 2-Degree of Freedom (DOF) IMC Proportional Integral Differentiator (PID) control, the input signal is 0.17 Nm in 1 s. It then increases to 0.2 Nm in 1.1s before decreasing to 0.15 Nm in 2.5 s. Subsequently, the control signal increases to 1.15 Nm and remains constant. For the proposed method, the control input signal is 0.15 Nm in 1 s. It slightly increases to 0.16 Nm in 1 s, and then the control input signal remains constant. The proposed control input is unaffected by disturbances.

Actual pipe positions were measured using proximity sensor. The simulation error of proposed technique is less compared with existing techniques. In the experimental results, the angle of the pipe increases to 8 ° in 2 s and then decreases to 0 in 3 s. Subsequently, the angle increases to 8 ° in 4 s, and the angle decreases to. The outcomes of the simulation and experiment are comparable, as is shown in Figure 11(a). Similarly, in the experimental results, the displacement of the pipe increases to 34 ° in 2 s and then decreases to 0 in 3 s. Afterward, the displacement increases to 340 in 4 s, and the displacement decreases to 0. The outcomes of the simulation and experiment are comparable, as shown in Figure 11(b). Furthermore, the angle of the pipe increases to 6 ° in 2 s and then decreases to

-3.8 ° in 3 s. After the angle increases to 4 ° in 4 s, the angle decreases to -5 °. The outcomes of the simulation and experiment are comparable, as is shown in Figure 11(a). The angle of the pipe increases to 12.4° in 2 s and the angle decreases to 1° in 3 s after the angle increases to 12.4° in 4 s and the angle decreases to 1°. Here, the "Blade Angle" elucidates the angular orientation of the cutting blade itself. The outcomes of the simulation and experiment are comparable as is shown in Figure 12(a). The angle of the pipe increases to 7° in 2 s and then it decreases to -1° in 3 s. Afterward, the angle increases to 7° in 4 s and finally, it decreases to -1° in the 2nd cycle. Here, we focus on the "Pipe Angle", representing the angular orientation of the entire pipe relative to a fixed reference frame. The outcomes of the simulation and experiment are comparable, as is shown in Figure 12(b). The angle of the pipe increases to 7.5° in 2 s and then it decreases to 0.5° in 3 s. Afterward, the angle increases to 7.5° 4 s, and finally, it decreases to 1° in the 3rd cycle. The outcomes of the simulation and experiment are comparable, as is shown in Figure 12(c).

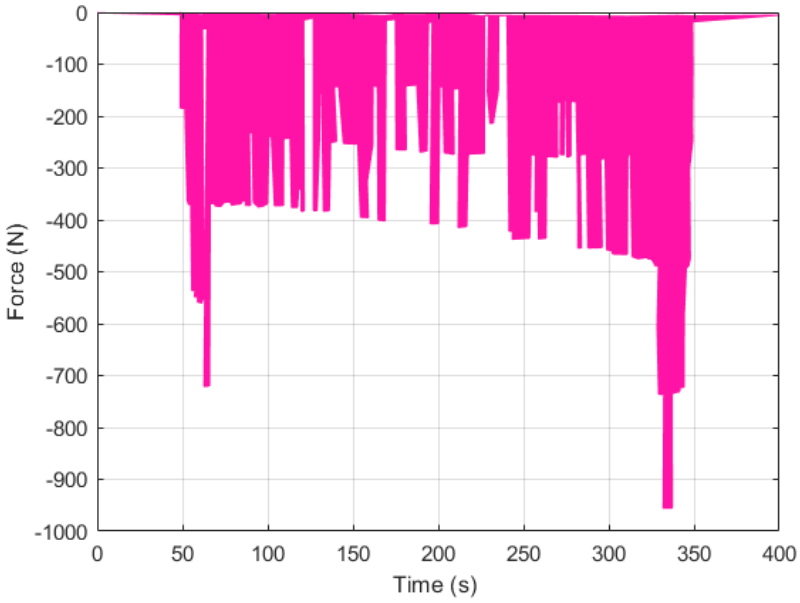

Figure 7. Pipe cutting machine force.

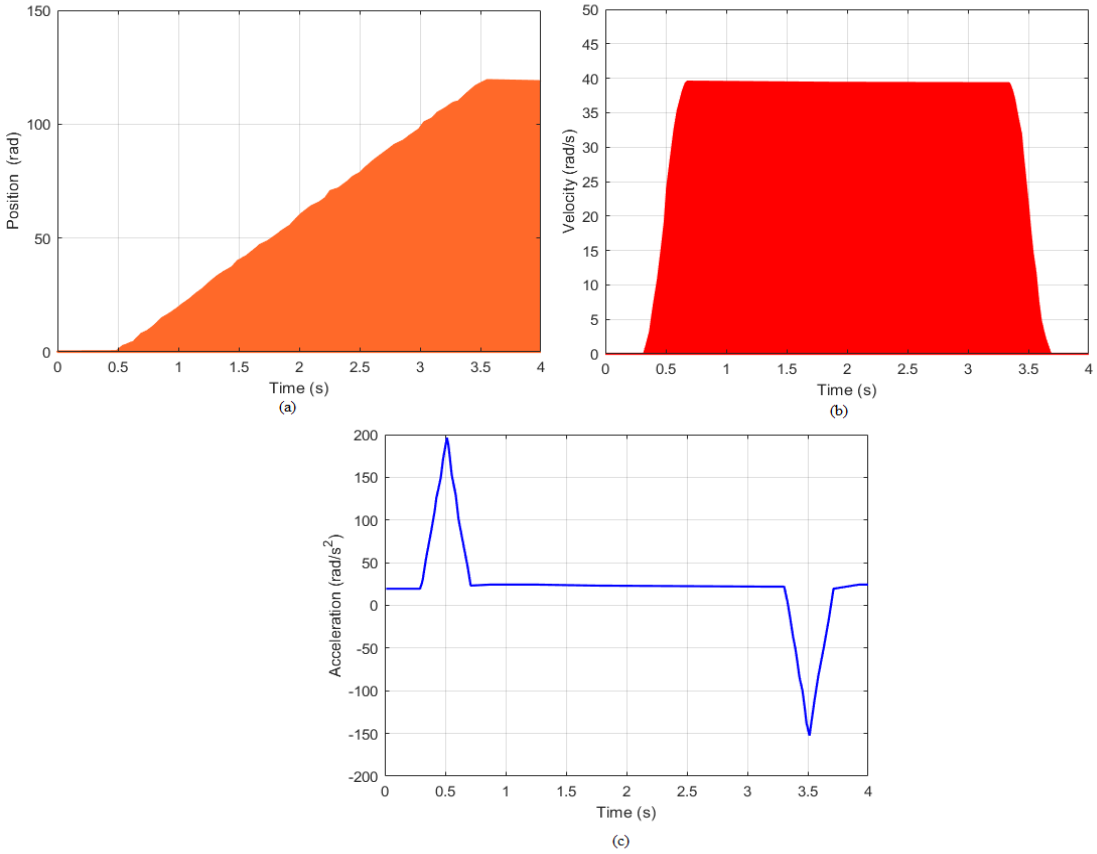

Figure 8. The cutting machine performance based on servo motor: (a) position of pipe, (b) velocity, and (c) acceleration.

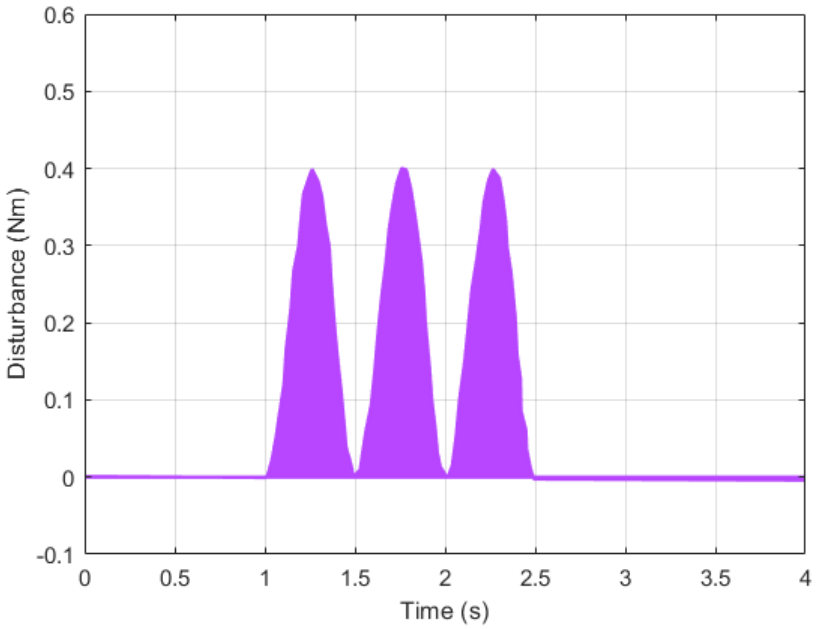

Figure 9. Tracking accuracy of the servo motor control.

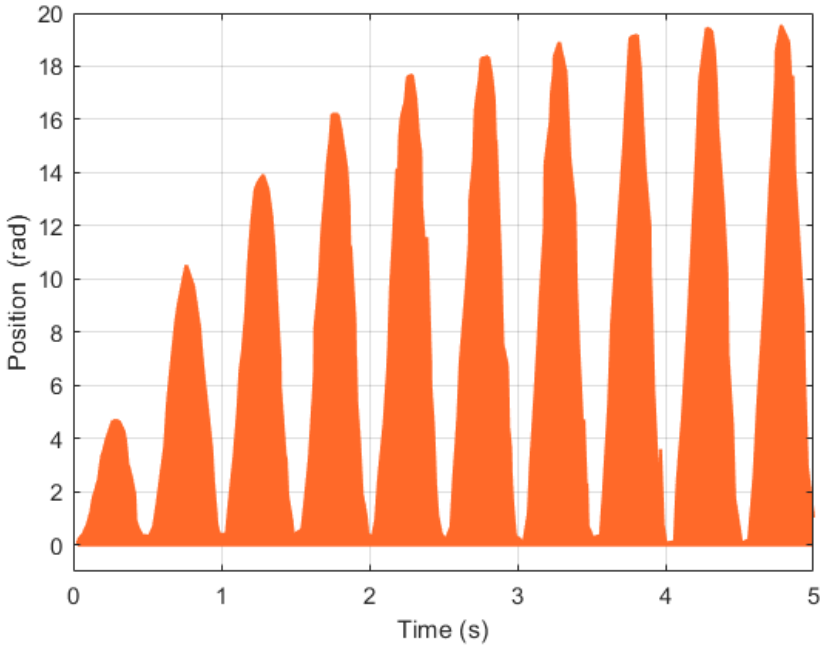

Figure 10. Robustness of servo motor based tracking position.

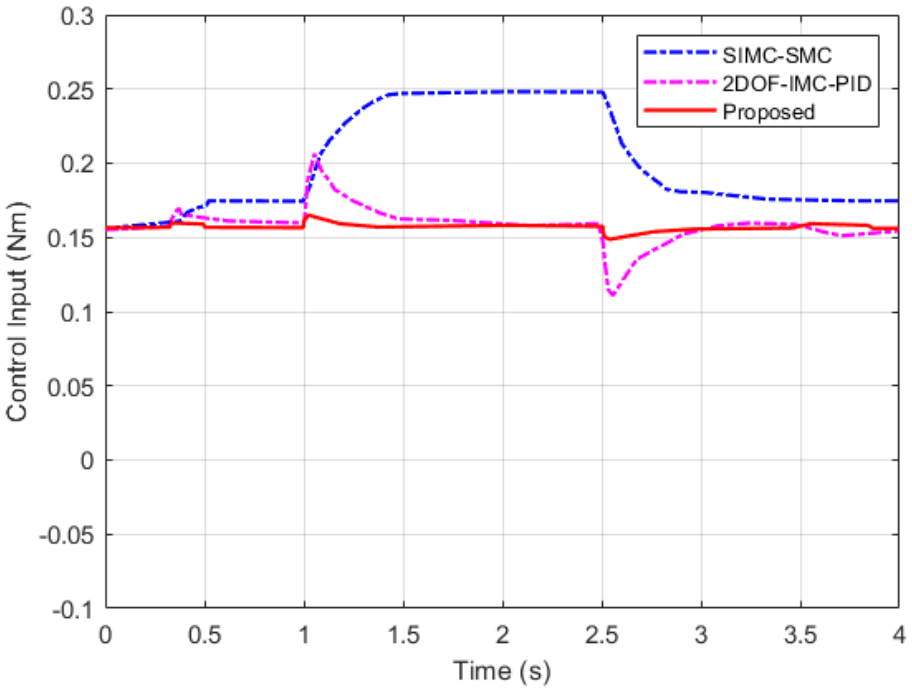

Figure 11. Position tracking errors with control input.

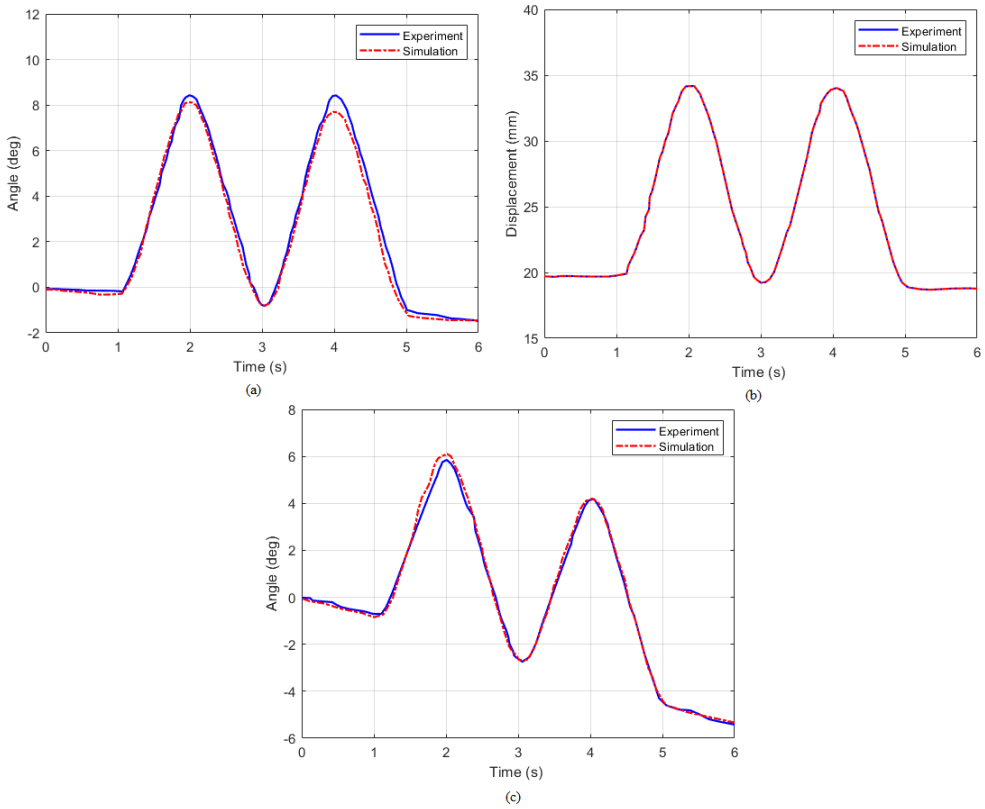

Figure 12. Position of the pipe: (a) pipe angle, (b) displacement, and (c) pipe angle.

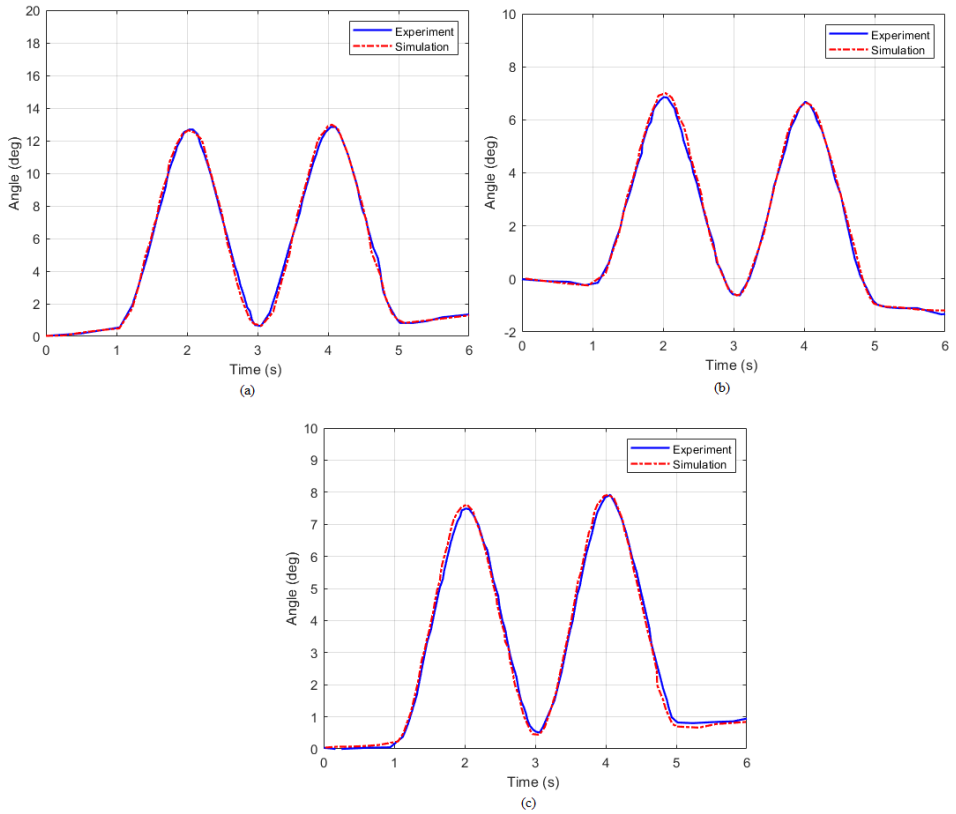

Figure 13. Proximity sensor showing position of pipe: (a) angle 1st position, (b) 2nd angle, and (c) 3rd angle.

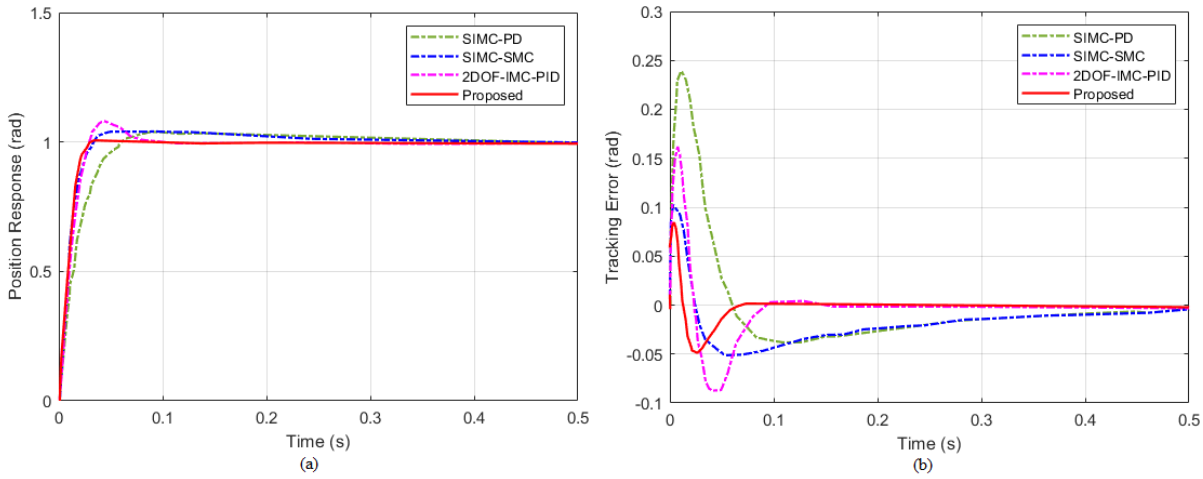

Figure 14. Step responses of servo motor: (a) position reaction and (b) error tracking.

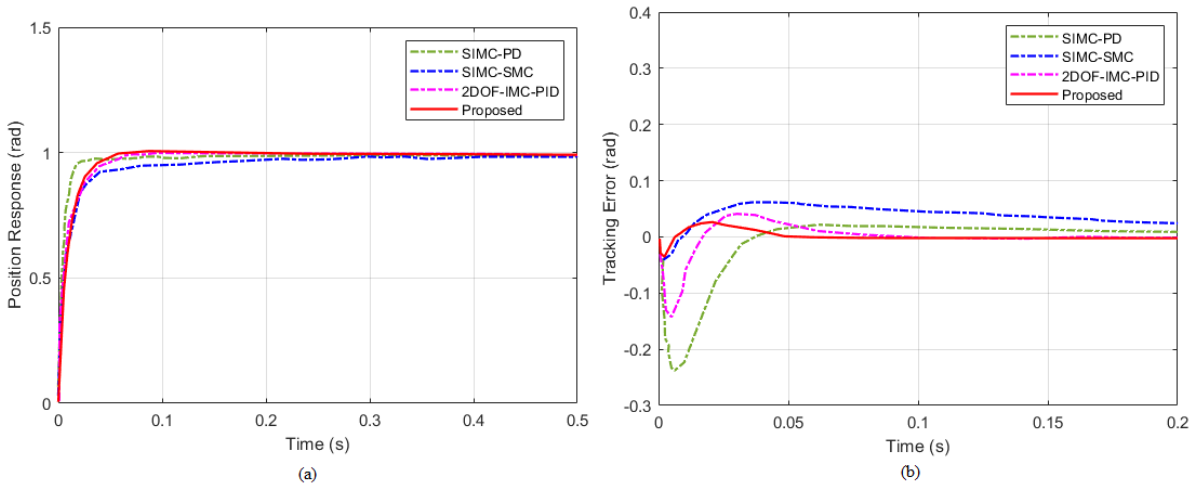

Figure 15. Step responses: (a) position reaction and (b) error tracking.

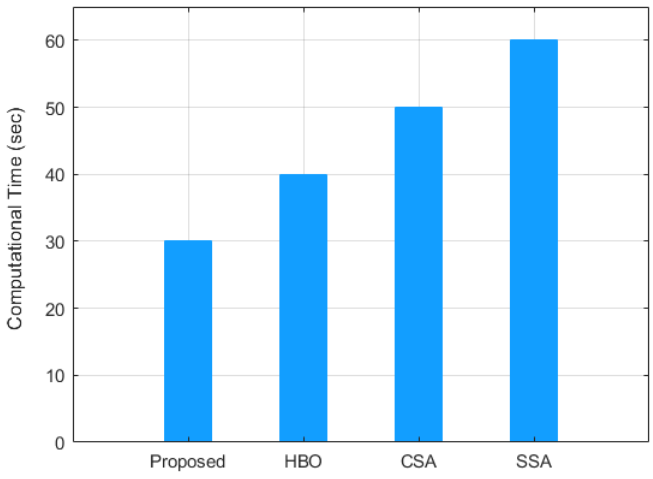

Figure 16. Comparison of computation time of proposed approach and existing approaches.

Table 2. Controller parameters.

Parameter	Specification
PLC type	PS4-201 MM1
Digital inputs	8
Digital outputs	6
Analog inputs (0-10 V)	4
Analog output (0-10 V)	1
Interface	RS232
Memory	32 kb

Table 3. Simulation parameter for the proposed system.

Parameter	value
Moment of inertia (J)	1.6×10^{-4} kg.m^2
Viscous friction coefficient (B)	0.001 Nm/(rad/s)
Target trajectory radius	300mm
Target trajectory velocity	7.5 deg/s
Maximum velocity	$v$max = 40 rad/s
Maximum acceleration	$a$max = 200 rad/s^2
Step disturbance	0.2Nm
Sinusoidal disturbance	$0.2[1 - \cos(12.56t)]$ Nm
Upper bound of the input disturbance	Dmax = 1 Nm

Table 4. Parameter table of APCNN.

Parameter	value
Number of pyramid levels (N)	3
Base CNN model	50-layer ResNet
Momentum	0.9
Minibatch size	16
Number of epochs	100
Initial learning rate	0.001

The position response of SIMC-PD increases from 0 to 0.9 rad in 0.4 s after it is constant the entire time. The position response of SIMC-SMC increases from 0 to 1 rad in 0.3 s and the position response is constant the entire time. The position response of 2DOF-IMC-PID increases from 0 to 1.1 rad in 0.3 s and the position response contains a slight decrease after it is constant the entire time. The position response of the proposed method increases from 0 to 1 rad in 0.3 s and the position response is constant the entire time, as is shown in Figure 13(a). The tracking error of SIMC-PD increases to 0.24 rad in 0.3 s and tracking error decreases to -0.03 rad in 0.1 s after tracking error is constant the entire time. The tracking error of SIMC-SMC is -0.05 rad in 0.15 s and tracking error slightly increases to 0. The 2DOF-IMC-PID has a tracking error of -0.15 rad in 0.5 s, which lowers to -0.07 rad and then climbs to 0. The tracking error of the proposed method is 0.4 rad and tracking error decreases -0.05 rad in 0.3 s and tracking error increases to 0 and remains constant as is shown in Figure 13(b). The position response of SIMC-PD increases from 0 to 0.9 rad in 0.4 s after it is constant the entire time. The position response of SIMC-SMC increases from 0 to 0.8 rad in 0.3 s and the position response is constant the entire time. The position response of 2DOF-IMC-PID increases from 0 to 0.9 rad in 0.3 s and the position response contains a slight decrease after it is constant the entire time. The position response of the proposed approach increases from 0 to 1 rad in 0.3 s and the position response is constant the entire time.

The position response of the proposed approach is high as is shown in Figure 14(a). The

tracking error of SIMC-PD decreases to -0.27 rad in 0.1 s and tracking error increases to 0 after tracking error is constant the entire time. The tracking errors of SIMC-SMC increases to 0.07 rad in 0.01 s, and the tracking errors are constant the entire time. After remaining constant for 0.1 s, the tracking error of 2DOF-IMC-PID climbs to 0.01 and then reduces to -0.13 rad. The tracking error of the proposed method increases 0.02 rad and tracking error slightly decreases to 0 after tracking error is constant the entire time, as is shown in Figure14(b). The computation time of the proposed system is compared with the existing system. Here, the computation time of HBO approach is 40 s, the CSA approach is 50 s, the SSA approach is 60 s, and the proposed system is 30 s. The proposed system computation time is low compared to the existing system approaches. Figure 15 shows step responses for (a) position reaction and (b) error tracking. Figure 16 shows the comparison of computation time of proposed approach and existing approaches. Controller parameters are shown in Table 2. Simulation parameters for the proposed system are depicted in Table 3. Parameter table of APCNN is presented in Table 4.

6. Conclusions

Here, the DAO-APCNN approach enhanced production efficiency by automating pipe cutting processes, which resulted in precise and consistent outcomes, with reduced reliance on manual labor and low cost productivity. An HMI can be used to handle and monitor the tool's operation. It has been successfully used to create an automated pipe-cutting machine using an AC servo motor and PLC. The pipe cutting force of the pipe cutting machine analyzed and the proximity sensor is determined for the accurate position of the pipe. The servo motor rotation is determined by the encoder and based on the rotation of the length of the pipe desired and accordingly the pipe cutting machine automatically cuts the pipe. The position tracking error is less compared with other approaches. The velocity and acceleration of the pipe cutting machine is also controlled by the servo motor. The result is low computation time compared with existing approaches. The computation time of the HBO is 40 s, the CSA approach is 50 s, the SSA approach is 60 s, and the proposed system computation time is 30 s. The proposed system computation time is low compared to the existing approaches. When the computation time is low, production efficiency is increased and cost is minimized.

Use of AI tools declaration

The authors declare that they have not used Artificial Intelligence (AI) tools in the creation of this article.

Conflict of interest

The authors declare that there are no conflicts of interest in this paper.

References

1. Franco JT, Buzatto HK, de Carvalho MA (2023) TRIZ as a Strategy for Improvement of Process Control in the Wood Industry. In *TRIZ in Latin America: Case Studies* 175–191. Cham: Springer International Publishing. https://doi.org/10.1007/978-3-031-20561-3_8

2. Ding Y, Ma Y, Liu T, Zhang J, Yang C (2023) Experimental Study on the Dynamic Stability of Circular Saw Blades during the Processing of Bamboo-Based Fiber Composite Panels. *Forests* 14: 1855. https://doi.org/10.3390/f14091855
3. Kim M, Lee SU, Kim SS (2021) Real-time simulator of a six degree-of-freedom hydraulic manipulator for pipe-cutting applications. *IEEE Access* 9: 153371–153381. https://doi.org/10.1109/ACCESS.2021.3127502
4. Chen Z, Zhang Y, Wang C, Chen B (2021) Understanding the cutting mechanisms of composite structured soft tissues. *Int J Mach Tool Manu* 161: 103685. https://doi.org/10.1016/j.ijmachtools.2020.103685
5. Wang H, Satake U, Enomoto T (2023) Serrated chip formation mechanism in orthogonal cutting of cortical bone at small depths of cut. *Journal of Materials Processing Technology* 319: 118097. https://doi.org/10.1016/j.jmatprotec.2023.118097
6. Wang Z, Li T (2022) Design of gas drainage system based on PLC redundancy control technology. https://doi.org/10.21203/rs.3.rs-2361008/v1
7. Paul A, Biradar B, Salkar T, Mahajan S (2023) Study on Various Type of Packaging Machines. *Grenze International Journal of Engineering & Technology (GIJET)* 9(2).
8. Peng C, Zhang Z, Liu W, Li D (2022) Ranking of Key Components of CNC Machine Tools Based on Complex Network. *Math Probl Eng* 2022. https://doi.org/10.1155/2022/6031626
9. Syufrijal S, Rif'an M, Prabumenang AW, Wicaksono R (2021) Design and implementation of pipe cutting machine with AC servo motor and PLC based on HMI. In *IOP Conference Series: Materials Science and Engineering* 1098: 042082. IOP Publishing. https://doi.org/10.1088/1757-899X/1098/4/042082
10. Wang G, Sun X, Luo Z, Ye T (2021) Cutting Device for Production of Spiral Submerged Arc Welded Pipe Based on PLC Control System. In *Big Data Analytics for Cyber-Physical System in Smart City: BDCPS, 28-29 2020, Shanghai, China* 901–906. Springer Singapore. https://doi.org/10.1007/978-981-33-4572-0_129
11. Rallabandi SR, Yanda S, Rao CJ, Ramakrishna B, Apparao D (2023) Development of a color-code sorting machine operating with a pneumatic and programmable logic control. *Materials Today: Proceedings*. https://doi.org/10.1016/j.matpr.2023.05.150
12. Attar KA, Patil SA, Patil PD, Sutar AD, Patil SA, Bartake G (2020) Development and Fabrication of Automatic Chakali Making Machine.
13. Talahma M, Isied O (2022) Design and Implement of a Prototyping Automatic Sweet Forming Machine.
14. Wu Q, Mao Y, Chen J, Wang C (2021) Application research of digital twin-driven ship intelligent manufacturing system: Pipe machining production line. *J Mar Sci Eng* 9: 338. https://doi.org/10.3390/jmse9030338
15. Yu M, Wang B, Ji P, Li B, Zhang L, Zhang Q (2023) Simulation analysis of the circular sawing process of medium density fiberboard (MDF) based on the Johnson–Cook model. *Eur J Wood Wood Prod* 1–3. https://doi.org/10.1007/s00107-023-02007-5
16. Shaheed BN, Selman NH (2023) Design and implementation of a control system for a steel plate cutting production line using programmable logic controller. *International Journal of Electrical and Computer Engineering (IJECE)* 13: 3969–3976. https://doi.org/10.11591/ijece.v13i4.pp3969-3976

17. Zhu H, Chen JW, Ren ZQ, Zhang PH, Gao QL, Le XL, et al. (2022) A new technique for high-fidelity cutting technology for hydrate samples. *Journal of Zhejiang University-SCIENCE A* 23: 40–54. https://doi.org/10.1631/jzus.A2100188
18. Zhu X, Zhong J, Jing J, Ye W, Zhou B, Shan H (2023) Fuzzy proportional–integral–derivative control system of electric drive downhole cutting tool based on genetic algorithm. *Proceedings of the Institution of Mechanical Engineers, Part E: Journal of Process Mechanical Engineering* 09544089231172608. https://doi.org/10.1177/09544089231172608
19. Du T, Dong F, Xu R, Zou Y, Wang H, Jiang X, et al. (2022) A Drill Pipe-Embedded Vibration Energy Harvester and Self-Powered Sensor Based on Annular Type Triboelectric Nanogenerator for Measurement while Drilling System. *Adv Mater Technol* 7: 2200003. https://doi.org/10.1002/admt.202200003
20. Mu X, Xue Y, Jia YB (2023) Dexterous Robotic Cutting Based on Fracture Mechanics and Force Control. *IEEE T Autom Sci Eng*. https://doi.org/10.1109/TASE.2023.3309784
21. Limonov L, Osichev A, Tkachenko A, Kunchenko T (2022) Dynamics of the Electric Drive of the Flying Saw of an Electric Pipe Welding Mill. In *2022 IEEE 3rd KhPI Week on Advanced Technology (KhPIWeek)* 1–6. IEEE. https://doi.org/10.1109/KhPIWeek57572.2022.9916384
22. Salem ME, El-Batsh HM, El-Betar AA, Attia AM (2021) Application of neural network fitting for pitch angle control of small wind turbines. *IFAC-PapersOnLine* 54: 185–190. https://doi.org/10.1016/j.ifacol.2021.10.350
23. Vadi S, Bayindir R, Toplar Y, Colak I (2022) Induction motor control system with a Programmable Logic Controller (PLC) and Profibus communication for industrial plants—An experimental setup. *ISA T* 122: 459–471. https://doi.org/10.1016/j.isatra.2021.04.019
24. Barbosa AF, Campilho RD, Silva FJ, Sánchez-Arce IJ, Prakash C, Buddhi D (2022) Design of a Spiral Double-Cutting Machine for an Automotive Bowden Cable Assembly Line. *Machines* 10: 811. https://doi.org/10.3390/machines10090811
25. Ali AW, Alquhali AH (2020) Improved Internal Model Control Technique for Position Control of AC Servo Motors. *ELEKTRIKA-Journal of Electrical Engineering* 19: 33–40. https://doi.org/10.11113/elektrika.v19n1.179
26. Vaishnavi Patil DP, Manjunath TC (2023) Design, Development of a Diversified Implemention of a Supervisory Control And Data Acquisition based VLSI System (SCADA) framework Utilizing Microcontroller based Programmable Logic Controllers. *Tuijin Jishu/Journal of Propulsion Technology* 44: 879–890. https://doi.org/10.52783/tjjpt.v44.i3.389
27. Acosta PC, Terán HC, Arteaga O, Terán MB (2020) Machine learning in intelligent manufacturing system for optimization of production costs and overall effectiveness of equipment in fabrication models. *Journal of Physics: Conference Series* 1432: 012085. IOP Publishing. https://doi.org/10.1088/1742-6596/1432/1/012085
28. Chengye L, Rui W, Wanjin W, Yajun W, Hao L, Xianmeng Z (2021) Development of Special Device for Cutting Irradiation Test Tube. *核动力工程* 42: 10–14.
29. Srinivas GL, Singh SP, Javed A (2021) Experimental evaluation of topologically optimized manipulator-link using PLC and HMI based control system. *Materials Today: Proceedings* 46: 9690–9696. https://doi.org/10.1016/j.matpr.2020.08.023
30. Zuo Y, Mei J, Zhang X, Lee CH (2020) Simultaneous identification of multiple mechanical parameters in a servo drive system using only one speed. *IEEE T Power Electr* 36: 716–726. https://doi.org/10.1109/TPEL.2020.3000656

31. Eshraghian JK, Wang X, Lu WD (2022) Memristor-based binarized spiking neural networks: Challenges and applications. *IEEE Nanotechnol Mag* 16: 14–23. https://doi.org/10.1109/MNANO.2022.3141443
32. Fuller A, Fan Z, Day C, Barlow C (2020) Digital twin: Enabling technologies, challenges and open research. *IEEE access* 8: 108952–108971. https://doi.org/10.1109/ACCESS.2020.2998358
33. Roozbahani H, Alizadeh M, Ahomäki A, Handroos H (2021) Coordinate-based control for a materials handling equipment utilizing real-time simulation. *Automat Constr* 122: 103483. https://doi.org/10.1016/j.autcon.2020.103483
34. Park CG, Yoo S, Ahn H, Kim J, Shin D (2020) A coupled hydraulic and mechanical system simulation for hydraulic excavators. *Proceedings of the Institution of Mechanical Engineers, Part I: Journal of Systems and Control Engineering* 234: 527–549. https://doi.org/10.1177/0959651819861612
35. Zhang Y, Ding W, Deng H (2020) Reduced dynamic modeling for heavy-duty hydraulic manipulators with multi-closed-loop mechanisms. *IEEE Access* 8: 101708–101720. https://doi.org/10.1109/ACCESS.2020.2998058
36. Zhu Z, Buck D, Guo X, Cao P, Wang J (2020) Cutting performance in the helical milling of stone-plastic composite with diamond tools. *CIRP J Manuf Sci Tech* 31: 119–129. https://doi.org/10.1016/j.cirpj.2020.10.005
37. Wang BJ, Lin CH, Lee WC, Hsiao CC (2023) Development of a Bamboo Toothbrush Handle Machine with a Human–Machine Interactive Interface for Optimizing Process Conditions. *Sustainability* 15: 11459. https://doi.org/10.3390/su151411459
38. Ding Y, Ma Z, Wen S, Xie J, Chang D, Si Z, et al. (2021) AP-CNN: Weakly supervised attention pyramid convolutional neural network for fine-grained visual classification. *IEEE T Image Process* 30: 2826–2836. https://doi.org/10.1109/TIP.2021.3055617

AIMS Press